FWI using Patched Green's Functions for target-oriented time-lapse inversion

Danyelle da Silva *; Edwin Fagua Duarte and Joao Medeiros de Araujo, Universidade Federal do Rio Grande do Norte.

Abstract

We develop a target-oriented scheme to perform time-lapse Full Waveform Inversion using a frequency domain wave propagator based on Patched Green's Functions (PGF). PGF is a well-known technique used in condensed matter physics to calculate the electronic wave field in materials with holes. Adapting this scheme to seismic wave propagation in the subsurface we obtain the same result as conventional FWI but significantly reducing the inversion time because we calculate the wave fields just in the target area. By simulated time-lapse experiments in a typical Brazilian pre-salt model, we demonstrate that the target-oriented PGF reduces the computational time of the inversion without compromising its accuracy. We illustrate this result by varying the velocity of the pre-salt reservoir, and use PGF FWI double-difference approach, to recover the time-lapse velocity variation that we introduced. We obtain a good result, comparable with the conventional FWI using a mask over the target area, but at a much reduced computational time. We also discuss the robustness of the results in the presence of an imperfect baseline velocity model.

Introduction

Time-lapse seismic monitoring of Brazilian pre-salt reservoirs has recently been demonstrated in Cypriano et al. (2019), and Kiyashchenko et al. (2020), and has provided the impetus for wider application. However, the process is expensive and time-consuming because of the cost of repeated acquisition of OBN surveys and processing of the 4D data, including through FWI.

In time-lapse seismic, it is necessary to retrieve information just from a target region i.e., the portion of the reservoir that is changing due to production processes. If conventional FWI is applied, it is mandatory to calculate the wave field in all domain, outside and inside the target.

Recently we have introduced a wave propagator based on the Patched Green Function (PGF) method (Moura et al., 2020; Barbosa et al., 2020) in order to calculate wave propagation on a target area. In condensed matter physics, the PGF method is used to calculate the electronic transport in solids such as nanoscale graphene waveguides (Power and Jauho, 2014; Settnes et al., 2015). One application of the PGF technique is the calculation of electron wave functions when holes are present in the graphene lattice.

By making an analogy between the carbon atoms on the graphene lattice and the discretized cells on a subsurface velocity model, our wave propagator calculates the wavefield inside a target area and in receiver positions by separating the target area from the entire model, updating the velocity in the target area and connecting it back to the rest of model.

In this work, we describe our method by showing how to use the PGF technique to calculate the wavefield inside the target and at receiver positions. This information is necessary to calculate the misfit and the gradient used to perform FWI. We simulate time-lapse seismic scenarios by varying the velocity in a representative portion of the pre-salt reservoir in our model, and use PGF FWI double-difference approach, to try to recover the velocity variation that we introduced. We obtain a good result, comparable with the conventional FWI approach where wave propagation occurs in the full spatial domain, although at a much reduced computational cost. To make the comparison more realistic, we use a mask to limit the conventional FWI updates to the same target area. We also discuss the impact of an imperfect baseline velocity model, as would be the case in practice.

Methodology

Conventional wave propagation

To perform the synthetic simulations in frequency domain FWI it is necessary to solve the Helmholtz equation. As shown in (Marfurt, 1984) and Virieux and Operto (2009), in a finite difference approximation, the Helmholtz equation becomes a linear system where the variables are the wavefield amplitudes. The resulting linear system can be expressed as (Marfurt, 1984)

$$\mathbf{G}^{-1}\psi = \frac{F_\omega}{h^2}\mathbf{U}^s, \tag{1}$$

where h is the cell size of the amplitude grid, F_ω is the Fourier coefficient of source wavelet for frequency ω, $\mathbf{U}^s$ is a vector with zero elements everywhere except on the source position s and G^{-1} is called the impedance matrix whose inverse is the Green's function (GF) associated with the wave equation. In other words, the matrix element G_{ij} describes the wave propagation between positions j and i.

Patched Green Functions

In target-oriented inversion schemes, it is possible to update the velocity model only in a small region of the

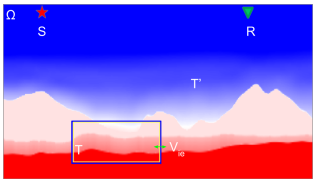

(a)

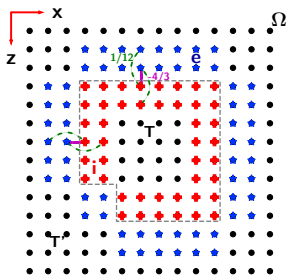

(b)

Figure 1: (a) A 2D system (velocity model) used to calculate the Green's Function. The subsystems T and T' initially disconnected, are connect by potential $\mathbf{V}_{ei}$ to form Ω. (b) Representation of potential $\mathbf{V}_{ie}$ using a fourth-order laplacian. The purple and green lines depict the coefficients of potential shown in equation 6. The dashed gray line represents the limit between target area T and outside target area T'.

subsurface, as would be the case of time-lapse monitoring. If conventional FWI is applied to this kind of problem, it is necessary to calculate the wave field for the entire computational domain using equation 1. To reduce the computational cost associated with the calculation of Green's functions, we apply the Patched Green Function method described in Moura et al. (2020), which uses Dyson's equation for the calculation of Green's function between the source and the receivers in the case of the wave velocities being modified only in a smaller region that will be considered as the destination area. The Dyson equation allows calculating the green function $\mathbf{G}$ of a system under a potential $\mathbf{V}$ when the Green's function of the unperturbed system $\mathbf{g}$ is known. The Dyson equation can be stated as

(Economou, 2006; Doniach and Sondheimer, 1974; Sheng, 2006)

$$\mathbf{G}^{-1} = \mathbf{g}^{-1} - \mathbf{V} \Rightarrow \mathbf{G} = \mathbf{g} + \mathbf{gVG} \tag{2}$$

To better understand the meaning of Green's functions $\mathbf{G}$, $\mathbf{g}$ and potential $\mathbf{V}$ in the context of wave propagation using the PGF method, we use the system depicted in Figure 1(a). The Ω system represents the entire computational domain. The subsystems T and T' represent the target area and outside the target, respectively, such that $T \cup T' = \Omega$ is satisfied.

The connection potential $\mathbf{V}$ depends on the set of points contained in the boundary that delimit the target area (yellow line - inner boundary) and outside the target area (blue line - outer boundary), as shown in figure 1(a). Because the number of points on the outer and inner boundary of the target area is much smaller than the total number of points in the entire computational domain, the potential $\mathbf{V}$ is highly sparse, and the term $\mathbf{gVG}$ in equation 2 requires just some sub-matrices of the full Green Function. As shown in Moura et al. (2020), the Green functions required for the FWI, i.e., from sources to receivers and from sources to the target, are calculated following the equations

$$\mathbf{G}_{es} = (\mathbb{1} - \mathbf{g}_{ee}\mathbf{V}_{ei}\mathbf{g}_{ii}\mathbf{V}_{ie})^{-1}\,\mathbf{g}_{es}, \tag{3}$$

$$\mathbf{G}_{ts} = \mathbf{g}_{ti}\mathbf{V}_{ie}\mathbf{G}_{es}, \tag{4}$$

$$\mathbf{G}_{rs} = \mathbf{g}_{rs} + \mathbf{g}_{re}\mathbf{V}_{ei}\mathbf{g}_{ii}\mathbf{V}_{ie}\mathbf{G}_{es}, \tag{5}$$

where subscripts e and i represent, respectively, the set points containing the outer and inner boundary of the target. $\mathbf{V}_{ie}$ is the non-zero submatrix of the potential $\mathbf{V}$ connecting the target and outside target areas. The subscripts r and s and t depict the receivers, sources, and target positions, respectively. The equations 3-5 depend on quantities calculated in the T and T' systems before connection. The Green's Function $\mathbf{g}_{ee}$, $\mathbf{g}_{es}$ and $\mathbf{g}_{ts}$ are calculated in the outside target area, and the Green's Function $\mathbf{g}_{ii}$ and $\mathbf{g}_{ti}$ are calculated in the target area.

The implementation of the Dyson equation is exact, not involving any approximation. Therefore, the values obtained through equations 3-5 are numerically equivalent to the case where the functions of Green $\mathbf{G}_{rs}$ and $\mathbf{G}_{ts}$are calculated using equation 1. As described in Moura et al. (2020), the connecting potential $\mathbf{V}_{ie}$ between a pair of the points on the inner boundary and outer boundary of the target, i.e, the potential that connects the subsystems T and T', depends on the finite differences discretization used. In this work, we use a fourth-order laplacian that defines the connecting potential as

$$V_{ie} = \begin{cases} -4/3 & \text{if } |i-e| = 1 \text{ in x or z direction}, \\ 1/12 & \text{if } |i-e| = 2 \text{ in x or z direction}, \\ 0 & \text{otherwise.} \end{cases} \tag{6}$$

As shown by the equation 6, the connecting potential $\mathbf{V}$ is different to the potential used in the Born-Like approximation which is proportional to term $\omega^2(c(\mathbf{x})^{-2} - c_0(\mathbf{x})^{-2})$, where $c_0(\mathbf{x})$ is the background velocity.

Target-Oriented Gradient Calculation

Because FWI is an iterative local optimization process, the misfit function and gradient must be calculated for each iteration (Pratt et al., 1998; Virieux and Operto, 2009). The misfit function is calculated with the simulated wavefield at receiver positions, and the gradient is calculated with the wavefield at depth positions where the velocity model is updated. Using the notation in Tao and Sen (2013) the misfit function Φ is calculated as (da Silva et al., 2021)

$$\Phi = \frac{1}{2}\sum_{\omega}\sum_{s}\sum_{r}\Delta u^{*}(\mathbf{r},\mathbf{s};\omega)\Delta u(\mathbf{r},\mathbf{s};\omega), \tag{7}$$

where

$$\Delta u(\mathbf{r},\mathbf{s};\omega) = F_{\omega}G(\mathbf{r},\mathbf{s};\omega) - d_{obs}(\mathbf{r},\mathbf{s};\omega) \tag{8}$$

is the misfit between the observed data d_{obs} and the calculated data $F_{\omega}G(\mathbf{r},\mathbf{s};\omega)$. The gradient of misfit function

is calculated as (Tao and Sen, 2013)

$$\frac{\partial \Phi}{\partial c(\mathbf{x})} = -\frac{2}{c(\mathbf{x})^3} \sum_{\omega} \sum_{s} \sum_{r} F_{\omega} \omega^2 G(\mathbf{x},\mathbf{s};\omega) G(\mathbf{x},\mathbf{r};\omega) \Delta u^*. \quad (9)$$

In equations 7 to 9, the vectors $\mathbf{s}$ and $\mathbf{r}$ represent shots and receivers positions, respectively. The Green's functions used in misfit and gradient calculations are obtained from equations 3 to 5. $G(\mathbf{r},\mathbf{s};\omega)$ is obtained from the matrix $\mathbf{G}_{rs}$ calculated in equation 5 and $G(\mathbf{x},\mathbf{s};\omega)$, and $G(\mathbf{x},\mathbf{r};\omega)$ are obtained from $\mathbf{G}_{ts}$ calculated in the equation 4.

The gradient calculation is performed in two phases. In the first phase, called *split-out*, we form the impedance matrix $\mathbf{g}_{T'}$ corresponding only to the outside target area. We apply a LU factorization on $\mathbf{g}_{T'}$ in order to calculate the terms $\mathbf{g}_{ee}$, $\mathbf{g}_{es}$, $\mathbf{g}_{rs}$. This implies that the cost of the split-out phase depends on the number of receivers, sources and points e at the outer boundary of the target. The split-out phase is performed once at the beginning of the inversion.

In the second phase, called *fill-in*, we calculate the terms $\mathbf{g}_{ii}$ and $\mathbf{g}_{ti}$ using the impedance matrix $\mathbf{g}_T$ related just to the target area. For small targets, the fill-in phase is computationally fast. With the calculations done in the two phases, the equations (3)-(5) are solved by matrix multiplication. We change the velocity values in the initial model with the values of trial velocity during the inversion. This is done by changing the term $\omega^2 h^2 / c_i^2$ at the diagonal just in the $\mathbf{g}_T$ matrix.

Numerical Experiments

To assess the effectiveness of the PGF target-oriented FWI we perform simulated time-lapse experiments in a realistic model that represents the features of a typical Brazilian pre-salt field, figure 2(a). The dimension of the model is 7000 m in the vertical dimension and 25000 m in the horizontal dimension with cell size equal to 20m in each dimension.

We perform time-lapse inversion using the Double-Difference Full Waveform technique (DDFWI), introduced by Watanabe et al. (2004). In the DDFWI approach the baseline and monitor dataset are combined to form a newly observed data d_{DDFWI} as

$$d_{DDFWI} = (d_{monitor} - d_{baseline}) + u_{baseline}, \quad (10)$$

where $d_{monitor}$ and $d_{baseline}$ are the observed data for monitor and baseline respectively, and $u_{baseline}$ is a synthetic dataset modeled on the velocity model obtained from the inversion of baseline dataset. With the modified observed data defined in equation 10, the misfit function is calculated as

$$\Phi_{DDFWI} = \frac{1}{2} ||d_{DDFWI} - u_{monitor}||^2, \quad (11)$$

where $u_{monitor}$ is the simulated data in the monitor inverted model.

We use the Brazilian pre-salt model in Figure2(a) as the baseline model. To generate the monitor model, we add a perturbation by increasing the wave velocity by 3% (or 150 m/s) in the reservoir under the salt layer as shown in the black rectangle in Figure 2(a). The perturbation is shown in Figure 2(b). In this case, the area of the inverted target

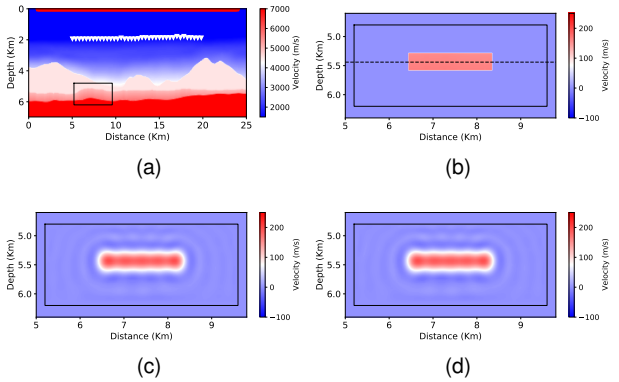

Figure 2: First scenario: baseline model is known perfectly. (a) Baseline velocity model representing a Brazilian pre-salt field. The red line at the top represents the sources and the white triangles the receivers positions at ocean bottom. The black rectangle is the target area used in the target inversion. (b) True Time- Lapse perturbation inside the target area. The dashed black line is the position of the profiles shown in Figure 4. (c) PGF inversion. (d) Inversion using conventional FWI with a mask.

corresponds to 3.5% ($10km^2$ approximately) of the entire velocity model ($175Km^2$ approximately).

For both baseline and monitor surveys, we simulate identical Ocean Bottom Node (OBN) acquisitions as shown in Figure 2(a). We simulate 576 shots at the surface with a source interval equal to 40m and deploy 38 receivers at the ocean bottom with a receiver interval equal to 400m. The spread for each shot was limited to have offsets less than 10km. The source signature is a Ricker wavelet with 5 Hz peak frequency and the record length and sample rate are 10 s and 20 ms, respectively. To avoid inversion crime, we modeled the observed data by using a wave propagator in the time domain.

Being the number of receivers smaller than the number of sources, we perform the inversion by interchanging the position of sources and receivers according to the principle of reciprocity for acoustic wave propagation (Aki and Richards, 2002; Virieux and Operto, 2009). We use the two versions of the baseline model (two scenarios described below) as the initial guess of the inversion and perform a multiscale strategy with two frequency bands: 1-5 Hz and 1-7 Hz in steps of 0.2 Hz inside each frequency band. We perform 30 iterations per frequency band.

We perform the inversion experiments in two scenarios. In the first scenario, we use as initial model the baseline model in Figure 2(a) simulating the ideal case where the baseline model is known exactly. In the second scenario we use a smoothed version of baseline as initial model to simulate the case where the baseline model is known only approximately, as would be the case when dealing with real field data.

Discussion

The inversions using the PGF combined with DDFWI methodology for first and second scenarios are shown in Figures 2(c) and 3(b), respectively. In both scenarios the time-lapse perturbation is well recovered. This agrees

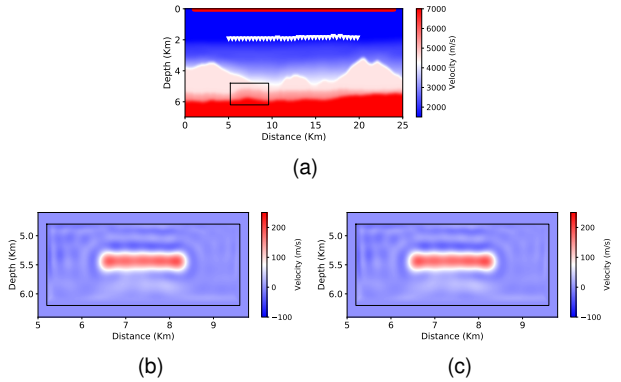

Figure 3: Second scenario: baseline model is known approximately. (a) Smoothed baseline velocity used to simulate a non-perfect initial velocity model. (c) PGF inversion. (c) Inversion using conventional FWI with a mask.

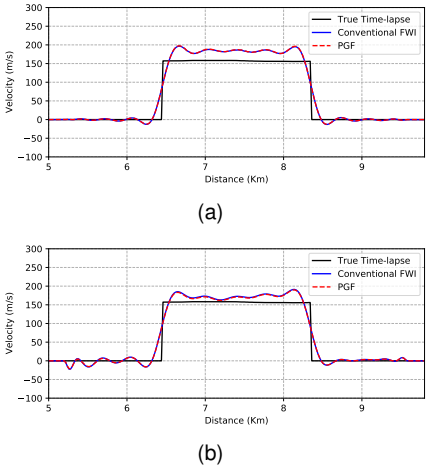

Figure 4: Horizontal velocity profile for inversion in the first scenario (a) with the exact baseline model, and in the second scenario (b) with an approximate baseline model.

with the discussion in Asnaashari et al. (2014), where the authors mentioned that the main advantage of the double-difference strategy is that the unexplained events that were not fitted during the inversion of the baseline data have low impact on the time-lapse perturbation inversion.

A common approach for target-oriented inversion using conventional FWI consists of applying a mask to update the velocity just in the target area. This constraint in the inversion focuses the updates in the area of interest, and does not allow updates outside this area. The results with conventional FWI using a mask for the first and second scenarios are shown in Figures 2(d) and 3(c), respectively. We found that the conventional FWI with a mask and the PGF FWI results are practically the same, as would be expected because of the theoretical equivalence between these two approaches. However, comparing the inversion times using these two methods (see Table 1), we see a significant reduction in inversion time for the PGF FWI method, as we expected.

Table 1: Relative time to perform DDFWI Time-Lapse inversion with conventional FWI and PGF method after sixty iterations.

Method	Time (%)
Conventional	100
PGF	32

Analyzing the horizontal velocity profiles in Figure 4, we notice a discrepancy between the magnitude of the perturbations recovered by inversions (around 180m/s) and the magnitude of the time-lapse perturbation in the model (150 m/s). This behavior is evidence of the Gibbs phenomenon since we are trying to invert a high-frequency perturbation with band-limited data. This phenomenon is similar to the observed in Virieux and Operto (2009), their Figure 6.

It is worth noting that, our synthetic experiments are performed in the absence of time-lapse noises that may arise from non-repeatability of the shot and receiver positions or variations in the velocities in the water layer between baseline and monitor surveys. In the case of real time-lapse data, where these types of noises are present, it is necessary to apply a preprocessing stage, where the baseline and monitor datasets are matched and filtered as shown, for example, in Kiyashchenko et al. (2011).

Conclusions

We propose a target-oriented FWI strategy in the frequency-domain for time-lapse surveys by using the Patched Green's Functions (PGF) method to calculate the wave field just in the target area and receivers positions. The objective to use the PGF method is to reduce the computational cost of FWI. This objective is accomplished because, in the PGF method, Green's functions necessary for the inversion are related to the target area, which is much smaller than the entire computational domain. Furthermore, the Green's functions associated with the outside area are calculated only once at the beginning of the inversion.

We test the PGF method combined with DDFWI in two scenarios, with exact and approximate baseline models, recovering the time-lapse perturbation for both scenarios. We obtain equivalent results using a conventional FWI approach with a mask applied in the target area, although at a much reduced computational time. Therefore, the PGF method appears as an attractive and robust alternative to inverting time-lapse datasets.

Future work to develop the PGF technique includes extension of the method to 3D geometries, more detailed analysis of the impact of imperfect baseline models, and application to field data.

Acknowledgements

The authors gratefully acknowledge support from Shell Brasil through the *New computationally scalable methodologies for target-oriented 4D seismic in pre-salt reservoirs* project at Universidade Federal do Rio Grande do Norte and the strategic importance of the support given by ANP through the R&D levy regulation.

References

Aki, K., and P. Richards, 2002, Quantitative seismology: University Science Books.

Asnaashari, A., R. Brossier, S. Garambois, F. Audebert, P. Thore, and J. Virieux, 2014, Time-lapse seismic imaging using regularized full-waveform inversion with a prior model: which strategy?: Geophysical Prospecting, **63**, 78–98.

Barbosa, W. A., E. F. Duarte, F. A. Moura, M. S. Ferreira, and J. M. de Araújo, 2020, Target-oriented wave propagator using the patched green function method: Presented at the 82nd EAGE Conference and Exhibition 2020, EAGE Publications BV.

Cypriano, L., Z. Yu, D. Ferreira, B. Huard, R. Pereira, F. Jouno, A. Khalil, E. Urasaki, N. da Cruz, A. Yin, D. Clarke, and C. Jesus, 2019, OBN for pre-salt imaging and reservoir monitoring – potential and road ahead: Presented at the Proceedings of the 16th International Congress of the Brazilian Geophysical Society&Expogef, Brazilian Geophysical Society.

da Silva, D., E. F. Duarte, W. Almeida, M. Ferreira, F. A. Moura, and J. M. de Araújo, 2021, Target-oriented inversion using the patched green's function method: GEOPHYSICS, **86**, R811–R823.

Doniach, S., and E. Sondheimer, 1974, Green's functions for solid state physicists: W. A. Benjamin. Frontiers in physics.

Economou, E., 2006, Green's functions in quantum physics: Springer. Springer Series in Solid-State Sciences.

Kiyashchenko, D., K. Mehta, J. Lopez, A. Maamari, R. Adawi, S. Busaidi, Y. Maskari, and G. Rocco, 2011, Time-lapse down-hole seismic surveys for deep EOR target monitoring in south oman: Presented at the SEG Technical Program Expanded Abstracts 2011, Society of Exploration Geophysicists.

Kiyashchenko, D., W.-F. Wong, D. Cherief, D. Clarke, Y. Duan, and P. Hatchell, 2020, Unlocking seismic monitoring of stiff reservoirs with 4d obn: A case study from brazil pre-salt: SEG Technical Program Expanded Abstracts 2020, 3759–3763.

Marfurt, K. J., 1984, Accuracy of finite-difference and finite-element modeling of the scalar and elastic wave equations: GEOPHYSICS, **49**, 533–549.

Moura, F. A., W. A. Barbosa, E. F. Duarte, M. S. Ferreira, J. M. de Araújo, and L. S. Lucena, 2020, Patched green's function method applied to acoustic wave propagation in disordered media: an interdisciplinary approach: Communications in Computational Physics.

Power, S. R., and A.-P. Jauho, 2014, Electronic transport in disordered graphene antidot lattice devices: Phys. Rev. B, **90**, no. 11, 115408.

Pratt, G., C. Shin, and Hicks, 1998, Gauss-newton and full newton methods in frequency-space seismic waveform inversion: Geophysical Journal International, **133**, 341–362.

Settnes, M., S. R. Power, J. Lin, D. H. Petersen, and A.-P. Jauho, 2015, Patched green's function techniques for two-dimensional systems: Electronic behavior of bubbles and perforations in graphene: Phys. Rev. B, **91**, no. 12, 125408.

Sheng, P., 2006, Introduction to wave scattering, localization and mesoscopic phenomena: Springer Berlin Heidelberg. Springer Series in Materials Science.

Tao, Y., and M. K. Sen, 2013, Frequency-domain full waveform inversion with a scattering-integral approach and its sensitivity analysis: Journal of Geophysics and Engineering, **10**.

Virieux, J., and S. Operto, 2009, An overview of full-waveform inversion in exploration geophysics: Geophysics, **74**, WCC1–WCC26.

Watanabe, T., S. Shimizu, E. Asakawa, and T. Matsuoka, 2004, Differential waveform tomography for time-lapse crosswell seismic data with application to gas hydrate production monitoring: Presented at the SEG Technical Program Expanded Abstracts 2004, Society of Exploration Geophysicists.